First-principles theory of surface magnetocrystalline anisotropy and the diatomic-pair model

Ding-sheng Wang
Department of Physics and Astronomy, Northwestern University, Evanston, Illinois 60208-3112 and Institute of Physics, Academia Sinica, Beijing 100080, China

Ruqian Wu
Department of Physics and Astronomy, Northwestern University, Evanston, Illinois 60208-3112

A. J. Freeman
Department of Physics and Astronomy, Northwestern University, Evanston, Illinois 60208-3112 and Materials Science Division, Argonne National Laboratory, Argonne, Illinois 60439

(Received 28 December 1992)

The state-tracking method proposed recently is employed for the first-principles determination of the magnetocrystalline-anisotropy (MCA) energy. A close relationship of the MCA energy to the band structure is found for transition-metal monolayers that show the change of sign of the MCA with respect to the band filling (atomic species) to be determined mainly by the spin-orbit coupling within the spin-down bands. The Fe monolayer with the π-bonding band as the highest occupied band exhibits positive MCA (easy axis along the layer normal). However, the effect of strain on the MCA of the Fe monolayer demonstrates the effect of the spin-orbit coupling between opposite-spin states. A model for the electronic origin of the magnetic anisotropy of this two-dimensional system is presented that explains the first-principles MCA results for iron and cobalt monolayers on the basis of the bonding character between two d atoms, the band broadening due to increase in coordination, and geometry (symmetry).

I. INTRODUCTION

Magnetocrystalline anisotropy (MCA) is one of the most important properties of ferromagnetic materials. Attempts to understand its microscopic origin started many years ago; work before 1960 was reviewed by Kanamori.[1] As proposed by Van Vleck[2] more than 50 years ago, the main contribution to the MCA is thought to originate from the relativistic spin-orbit coupling interaction (SOC), $H^{sl}=\xi\sigma\cdot\mathbf{L}$. When electron states with different orbital character are split due to the hybridization with neighboring atoms in a lattice and populated differently, their interaction with the spin (magnetic moment) gives rise to the anisotropy of its ground-state energy. The magnetic dipole and other possible anisotropic exchange interactions are usually found to play minor roles in determining the MCA.

The theoretical treatment for rare earths, where the SOC is much greater than the crystalline field, is quite successful in predicting the MCA energy and its temperature dependence,[3] even though a mean-field approximation is adopted for the description of the exchange interaction and a point-charge model is used for calculating the existing crystalline field.

In transition metals (TM) and their alloy systems, since the SOC is smaller than the crystalline field experienced by the rather extended $3d$ magnetic moments, the theoretical treatment of the MCA becomes much more difficult and still remains a great challenge even today. Earlier efforts in the 1960s and 1970s, based on the empirical or non-self-consistent band results for Fe, Ni, and Co crystals,[4–9] have taken hybridization and the SOC between the hybridized states into account. Work has also been extended to more complex systems, e.g., alloys.[10] The basic difficulty in the treatment of MCA in TM systems, as demonstrated in these studies, is that the MCA contribution of different Bloch states varies strongly over the Brillouin zone (BZ) and may become almost singular in the neighborhood of some k points. Hence, the treatment depends strongly on details of the band structure of each specific material and is thus quite tedious. The relationship between the MCA of even Fe, Ni, or Co with their electronic structure is not well understood.

Since the late 1970s, important advances in local spin-density electronic structure theory and dramatic enhancements of computational power took place; for example, the magnetic moment was determined for the first time for TM from first principles[11] and recently the total energy was calculated to better than about 0.01 eV, which makes possible the first-principles determination of the magnetic configuration for many complex artificial systems.[12] On the other hand, recent experiments successfully synthesized a large number of almost ideal artificial structures and revealed that many overlayer and superlattice systems show peculiar magnetic anisotropic properties (due to their reduced dimensionality and tailored structures on the atomic scale) that appear to be promising candidates for high-density magneto-optical storage media[13,14] and other applications. While these advances renewed interest in the theoretical understanding of the MCA for $3d$ TM, the fundamental problem is still how the MCA of magnetic atoms is determined by the symmetry and species of its neighboring atoms. Thus, it is strongly desired that *ab initio* calculations be

0163-1829/93/47(22)/14932(16)/$06.00

developed to explain the underlying physics and more importantly, predict new systems with desired properties in advance of experiments.

Such investigations have been made on either bulk crystals,[15–17] monolayers,[18–21] or thin films and multilayer structures.[22,23] Since they are based on state of the art first-principles band-structure methods, they are expected to produce better results for the MCA energy and provide an understanding of its mechanism. In TM systems, however, the SOC is extremely weak and the MCA energy is very small (about 10^{-6} eV/atom for highly symmetric cubic crystals and about 10^{-4} eV/atom for ultrathin films or monolayer systems). Thus, this energy is very small and so a perturbative (rather than self-consistent) treatment based on a force theorem[24] is always adopted, in which the SOC induced change of the total energy is approximated by the difference of the single-state energies summed over all occupied states, namely

$$E^{sl}=E(H^0+H^{sl})-E(H^0)=\sum_{i\in O'}\epsilon_i'-\sum_{i\in O}\epsilon_i \ . \tag{1}$$

The force theorem requires the condition that the perturbed and unperturbed occupied states have similar charge (spin) densities, so that the contribution from Coulomb and exchange-correlation terms in the total energy can be neglected. Here the prime denotes SOC perturbed states, energies, etc., and $O=\{o\}$ is the set of unperturbed occupied states and $O'=\{o'\}$ the set of SOC perturbed occupied states. In addition to the basic difficulty caused by the existence of the almost singular contribution at some k points experienced in earlier empirical treatments, another source of uncertainty and error is introduced when the sets of O and O' are determined independently by Fermi filling of the self-consistent energy spectrum ϵ_i and the non-self-consistent perturbed spectrum, ϵ_i'.[25] This makes the interpretation and theoretical determination of the MCA energy for the $3d$ TM from first principles have even more uncertainties than previous empirical treatments, despite the great advances in present day electronic structure theory and computational abilities.

In a previous paper,[25] we developed a state tracking method for the *ab initio* determination of the MCA energy from first-principles local-density electronic structure. By defining the occupation of the SOC perturbed states according to their wave functions instead of their eigenenergies, the state tracking perturbed occupied states $\{o'\}$ give the spatial distribution of the charge and spin densities as close as possible to the unperturbed $\{o\}$. This ensures the best application of the force theorem and the change between the two sets of occupied states reflects solely the physical effect of the SOC, free from uncertainties introduced in the non-self-consistent perturbation. This permits stable and precise results to be achieved with a substantially reduced number of integration k points, as shown in test calculations for free-standing Fe monolayers.

This paper presents expanded MCA results on strained Fe(001) monolayers and presents a model that explains its origin through the anisotropy of the SOC energy of a pair of d atoms. We begin in Sec. II from a general discussion of the SOC in connection with the MCA energy of the TM which emphasizes the difference between the MCA contributions from the SOC between the spin-down states and the SOC between opposite-spin states. This is followed by a model analysis of the magnetic anisotropy based on the bonding properties of a diatomic pair in Sec. III. After a description of the spin-polarized band structure of Fe monolayers as given by our highly precise full potential linearized augmented plane-wave (FLAPW) method,[26] the single-state SOC shift, the distribution in k space of the MCA contribution, the problem of the singular MCA contribution that occurs at some k points, the SOC induced energy and the resulting MCA are given in Sec. IV and compared, as a function of band filling, with the anisotropy model of the diatomic SOC energy. Finally, the effect of strain on the MCA energy of free-standing Fe monolayers is presented in Sec. V for different lattice spacings in a range of $\pm 10\%$ around the ideal bulk crystal value; it is then followed by conclusions in Sec. VI.

II. BACKGROUND PERSPECTIVE AND APPROACH

A. Perturbation theory analysis

As given in the relativistic theory, the SOC perturbed Hamiltonian is expressed by

$$H=H^0+H^{sl}=H^0+\xi(r)\boldsymbol{\sigma}\cdot\mathbf{L} \ , \tag{2}$$

where the SOC amplitude is

$$\xi(r)=\frac{1}{4c^2r}\frac{\partial V}{\partial r} \ . \tag{3}$$

For Fe $3d$ states its integrated value is about 30 meV, i.e., much smaller than that for rare-earth atoms, because of the weaker Coulomb potential, but the d bandwidth, a measure of the crystalline part H^0, is in the range 2–4 eV. As a result, any analysis that considers the SOC as a perturbation is justifiable for transition metals.

In the first order of perturbation, the energy shift of all states is identically zero because the diagonal elements of the SOC matrix vanish due to the time-reversal symmetry of the unperturbed states. Thus, the lowest-order contribution to the SOC induced change in the total energy comes in second order:

$$E^{sl}=\sum_o\sum_j\frac{|\langle o|H^{sl}|j\rangle|^2}{\delta\epsilon_{oj}} \ , \tag{4}$$

where o represents an occupied state and j is summed over all states and $\delta\epsilon_{oj}=\epsilon_o-\epsilon_j$. However, when j is also an occupied state, the two terms arising from the exchange of o and j cancel each other, and so the net contribution to the SOC induced energy comes solely from the interaction between the occupied and empty (u) states. This gives

$$\begin{aligned}E^{sl}(\boldsymbol{\sigma})&=-\sum_{o,u}\frac{|\langle o|H^{sl}|u\rangle|^2}{\delta\epsilon_{uo}}\\&=-(\xi)^2\sum_{o,u}\frac{|\langle o|\boldsymbol{\sigma}\cdot\mathbf{L}|u\rangle|^2}{\delta\epsilon_{uo}} \ .\end{aligned} \tag{5}$$

Here the SOC constant ξ is the radial integral of the product of the SOC amplitude $\xi(r)$ and the radial wave functions of states o and u. Since this integral is an atomic property that depends only on the derivative of the potential in the region near the nucleus, it does not vary very much even from the free atom to the solid.[27] Hence in the above expression, it is assumed constant for all d orbitals.

It is easy to see that this second-order perturbation expression and the constant radial integral approximation gives only isotropic contributions for cubic crystals where H^0 is invariant under the O_h group. As a result, a proper description of the MCA of cubic systems has to go to fourth order. However, this second-order expression is appropriate in describing the MCA energy of a pair of atoms, monolayers, and ultrathin films, as these have reduced symmetry and the second-order term dominates. some recent calculations of the MCA of films[28,29] were made by using the perturbation expression Eq. (5) and empirical electronic structure parameters. We should note that the analysis based on Eq. (5) given in this and the following sections is only used to help interpret our first-principles results which both solve the Schrödinger equation, including the SOC terms, accurately and include the complexity existing in a real physical system.

B. General formulation: Contribution of the coupling between parallel and opposite spin states

For the purpose of understanding the MCA mechanism for the iron group ferromagnets, it is very helpful to distinguish the contributions from the SOC between the parallel spin states and the SOC between the opposite spin states because, as shown below, they are comparable in many cases and behave differently. We may consider, as a good approximation, in the limiting case of strong exchange splitting that the spin-up band is almost fully occupied, and all empty states belong to spin-down bands. When the effect of the empty spin-up states is neglected, only two types of SOC have to be considered in the summation of Eq. (5), namely, the coupling between spin-down states, and the coupling between occupied spin-up states and empty spin-down states. The total SOC energy is approximately equal to the sum of the two contributions:

$$E^{sl}(\boldsymbol{\sigma}) \sim E^{dd}(\boldsymbol{\sigma}) + E^{ud}(\boldsymbol{\sigma}) , \tag{6}$$

where superscripts dd and ud represent the two types of SOC, and

$$E^{dd}(\boldsymbol{\sigma}) = -(\xi)^2 \sum_{o^-,u^-} \frac{|\langle o^-|L_\sigma|u^-\rangle|^2}{\delta\epsilon_{u^- o^-}} , \tag{7}$$

$$E^{ud}(\boldsymbol{\sigma}) = -(\xi)^2 \sum_{o^+,u^-} \frac{|\langle o^+|L_\sigma^-|u^-\rangle|^2}{\delta\epsilon_{u^- o^+}} , \tag{8}$$

where $o^+(u^+)$ and $o^-(u^-)$ represent occupied (empty) spin-up and spin-down states, respectively. The difference between the SOC energies for two magnetization directions also contains two terms,

$$\Delta E^{sl} = E^{sl}(\boldsymbol{\sigma}) - E^{sl}(\boldsymbol{\sigma}') \sim \Delta E^{dd} + \Delta E^{ud} . \tag{9}$$

According to Eq. (5), it is easy to show that if the two magnetization directions are perpendicular to each other, say z and x,

$$\Delta E^{dd} = E^{dd}(x) - E^{dd}(z) = (\xi)^2 \sum_{o^-,u^-} \frac{|\langle o^-|L_z|u^-\rangle|^2 - |\langle o^-|L_x|u^-\rangle|^2}{\epsilon_{u^-} - \epsilon_{o^-}} , \tag{10}$$

but

$$\Delta E^{ud} = E^{ud}(x) - E^{ud}(z) = (\xi)^2 \sum_{o^+,u^-} \frac{|\langle o^+|L_x|u^-\rangle|^2 - |\langle o^+|L_z|u^-\rangle|^2}{\epsilon_{u^-} - \epsilon_{o^+}} . \tag{11}$$

It is seen from Eqs. (10) and (11) that the contributions from two occupied states, with the same spatial wave function but different spin, are opposite in sign and will cancel each other. In the limit of zero exchange splitting, it gives vanishing anisotropy, as expected.

Since both ΔE^{dd} and ΔE^{ud} are summed over the spin-down empty states, they will certainly depend on the number of spin-down electrons (band filling), but their band filling dependence is different. ΔE^{dd} is not only determined by the orbital character of the occupied states, but it depends on the coupling with the empty states and also strongly on the splitting between them through the energy denominator in Eq. (10). It is sensitive to the change of the structure of the spin-down band. By contrast, the contribution from opposite spin states, ΔE^{ud}, is less dependent on the band structure. This is shown by assuming the energy denominator in Eq. (11) to be replaced by a constant $\Delta E_{\rm ex}$ and o^+ to be summed over the whole band. Simple mathematical manipulations give

$$E^{ud}(\boldsymbol{\sigma}) = -\frac{\xi^2}{\Delta E_{\rm ex}} \sum_{u^-} \langle u^-|L^2 - L_\sigma^2|u^-\rangle = \frac{\xi^2}{\Delta E_{\rm ex}} \left\{ -\frac{2}{3}(2l+1)l(l+1) + \sum_{o^-} \langle o^-|L^2 - L_\sigma^2|\bar{o}\rangle \right\} \tag{12}$$

Thus, for an axially symmetric system, with z denoting the symmetry axis and x an arbitrary direction in the perpendicular plane,

$$\Delta E^{ud} = E^{ud}(x) - E^{ud}(z) = \frac{\xi^2}{\Delta E_{\rm ex}} \sum_{o^-} \langle o^-|\tfrac{1}{2}(3L_z^2 - L^2)|o^-\rangle . \tag{13}$$

Under the assumptions given above, the sign of ΔE^{ud} depends only on the axial component of the angular momentum of the occupied states; its magnitude is inversely proportional to the exchange splitting, and it shows no relation to the separation or coupling between

states. According to Eq. (13), for this axially symmetric system, three states ($L_z=0,\pm1$) give negative contributions and two ($L_z=\pm2$) contribute positively. The maximum MCA due to this term may reach $\pm6\xi^2/\Delta E_{ex}$ per atom when, e.g., all occupied states give positive (negative) contributions.

The above general formulation, in not being dependent on the specific electronic structure, shows how various factors may affect the MCA. In the theoretical calculations, we have the freedom to switch the SOC on and off between different spin states separately, to change the band filling over a wide range, and to compare the results obtained with various physical pictures. This approach will be seen to be very useful in understanding the origin and the variation of the MCA as shown in the model discussed in Sec. III, in the interpretation of the first-principles results in Sec. IV, and in the explanation of the strain effect in Sec. V.

III. DIATOMIC-PAIR MODEL

It is well known from the phenomenological statistical theory[30] of magnetic annealing, and its experimental verification, that in TM alloys the directional ordering (preferential orientation) of atom pairs contributes substantially to the field-induced MCA. In this theory, the energy of a pair of atoms, either the same or different, is assumed to be dependent on the moment direction with respect to the pair axis. However, to our knowledge, no attempt has been made to elucidate the microscopic origin of this directionality with respect to the electronic states or bonding characteristics of the atoms, or to carry out theoretical calculations for any specific atomic pairs. Thus, it is not yet clear whether this magnetic anisotropy of atomic pairs, which plays so crucial a role in magnetic annealing, is related to the microscopic origin of the magnetic anisotropy in crystal ferromagnets. In this section, we explain how the dependence of the diatomic SOC energy on the moment direction is related to the electronic structure from the point of view of the second-order perturbation analysis described above, and present results about the monolayer MCA based on the model which includes this dependence, the effect of the geometry (symmetry), and the effect of band broadening with increase of the coordination number in a square lattice. In Sec. IV it is shown that this diatomic-pair model gives a good interpretation of the first-principles results of the MCA energy of Fe monolayers.

Let us start with a pair of two identical d atoms. When they are brought together, the hybridization of their d-electron orbitals leads to the formation of various bonding or antibonding states. Only the spin-down states are shown in Fig. 1 for simplicity; the spin-up states (not shown in the plot) are assumed to be located below these bands by an energy ΔE_{ex} due to the exchange splitting and to be fully occupied. The pair axis connecting the two atoms is denoted by PA. The strongest interaction, $V_{dd\sigma}$, gives the lowest bonding and the highest antibonding states separated by $2|V_{dd\sigma}|$, while the weakest interaction $V_{dd\delta}$, forms two doubly degenerate δ-bonding and antibonding states with the smallest separation, $2|V_{dd\delta}|$. Similarly there are also two degenerate π orbitals. In this simplest picture, the shift of the center of gravity of the hybridized d levels is omitted. Now, it is generally true that

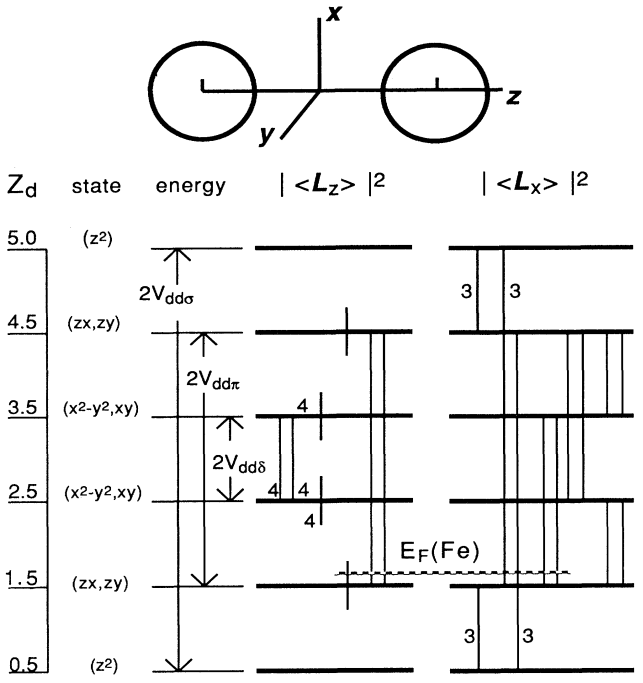

FIG. 1. Nonvanishing angular momentum matrix elements (solid vertical lines) between the d levels (thick horizontal lines) of a diatomic pair consisting of two identical atoms. The square of the corresponding elements equals 1 (not marked), 3, or 4 (marked by numbers beside the coupling lines). Z_d is the number of spin-down electrons when the corresponding levels are occupied. The approximate position of the Fermi levels of magnetic Fe atoms are drawn as dashed horizontal line.

$$|V_{dd\sigma}|>|V_{dd\pi}|>|V_{dd\delta}|\ , \tag{14}$$

as seen from the angular distribution of the atomic orbitals which determine the extent of the overlap. According to Harrison,[31] $|V_{dd\pi}|\sim0.54|V_{dd\sigma}|$, and $|V_{dd\delta}|$ is much smaller. Note that due to symmetry property of the atomic orbitals, only a few angular momentum matrix elements between the d orbitals are nonzero; they are given in Table I for the L_x, L_y, and L_z operators, and plotted for L_z and L_x matrix elements in Fig. 1 by vertical lines connecting corresponding levels. Double lines between degenerate states mean two nonvanishing matrix elements. Numbers beside these lines are the square of the matrix elements (cf. Table I). The contribution to the SOC induced energy is proportional to these values in second-order perturbation theory according to Eq. (5).

For the purpose of calculating $E^{dd}(\sigma)$, we only need to count those couplings which are between the occupied and empty spin-down states. Other couplings, either between the occupied spin-down states or between the empty spin-down states, contribute zero to this order of approximation. All contributions are enumerated in Table II for the magnetization along the pair axis E^{dd}(PA) and

TABLE I. Nonvanishing angular momentum matrix elements between d states. The notation is given for the d states in Cartesian coordinates with z as the quantization axis and for a square lattice monolayer in the band notation.

Matrix elements		
Cartesian	Band notation	$\langle L_\sigma \rangle$ value
$\langle xz\|L_z\|yz\rangle$	$\langle 5''\|L_z\|5'\rangle$	1
$\langle x^2-y^2\|L_z\|xy\rangle$	$\langle 3\|L_z\|4\rangle$	2
$\langle z^2\|L_x\|yz\rangle$	$\langle 1\|L_x\|5'\rangle$	$\sqrt{3}$
$\langle xy\|L_x\|xz\rangle$	$\langle 4\|L_x\|5''\rangle$	1
$\langle x^2-y^2\|L_x\|yz\rangle$	$\langle 3\|L_x\|5'\rangle$	1
$\langle z^2\|L_y\|xz\rangle$	$\langle 1\|L_y\|5''\rangle$	$\sqrt{3}$
$\langle xy\|L_y\|yz\rangle$	$\langle 4\|L_y\|5'\rangle$	1
$\langle x^2-y^2\|L_y\|xz\rangle$	$\langle 3\|L_y\|5''\rangle$	1

along an arbitrary perpendicular direction, i.e., in the plane perpendicular to the pair axis E^{dd}(PP). As a summation over both occupied and empty states, E^{dd} will obviously depend on the position of E_F or the number of spin-down d electrons, Z_d. Of course, at zero occupation of the spin-down band it is zero, and it is also zero when the band is fully occupied because the SOC operator is traceless. The magnitude of the induced energy depends on the SOC constant through a factor $-(\frac{1}{2}\xi)^2$ (the factor $\frac{1}{2}$ comes from the fact that each state consists of the orbitals of two atoms). E^{dd}(PA) is determined by the couplings between the bonding and antibonding states of either the δ or π bond, and is inversely proportional to the δ- and π-bonding strength through the energy denominator (see fourth column in Table II). However, E^{dd}(PP) is determined by the couplings among the δ, π, and σ states, and their differences play the crucial role (see second column in Table II).

A comparison between the two SOC energies E^{dd}(PA) and E^{dd}(PP) gives the inequalities listed in the third column in Table II. Note that these inequalities hold only if the bonding strength is in the order given by Eq. (14), which is generally believed to be true. At different band filling, the coupling between different (o,u) pairs of states contributes to $E^{dd}(\sigma)$; hence, the inequalities change direction for different band filling. A general relation about the anisotropy ΔE^{dd} of the diatomic SOC energy is thus drawn that when the spin-down d states are half occupied, E^{dd}(PA) $< E^{dd}$(PP) and the magnetic moment will prefer to lie along the pair axis; otherwise, E^{dd}(PP) $< E^{dd}$(PA) and the easy direction prefers the perpendicular plane. Numerical results are given in the top panel of Fig. 2 for a typical choice of parameters, i.e., $V_{dd\sigma}=-0.25$ eV, $V_{dd\pi}=0.18$ eV, $V_{dd\delta}=-0.04$ eV, and $\xi=30$ meV, in accordance with that given later in Sec. IV for the Fe monolayer with a square lattice constant $a=5.98$ a.u. The inequalities shown in Table II and the change of sign of this MCA property are clearly shown in this figure. For this diatomic pair, as shown in Fig. 2, the anisotropy contribution ΔE^{dd} is as large as 10 meV.

The contribution from the SOC between opposite-spin states, $E^{ud}(\sigma)$, has also been calculated using Eq. (11) with the same bonding parameters and an exchange splitting $\Delta E_{\rm ex}=3.0$ eV, also taken from the self-consistent Fe monolayer results. It is plotted in the bottom panel of Fig. 2, and an anisotropy contribution is clearly shown to exist that when the spin-down band is less than half occupied, E^{ud}(PP) $< E^{ud}$(PA), and when the spin-down band is more than half occupied, E^{ud}(PP) $> E^{ud}$(PA). This behavior is determined by the fact that the bonding σ and π orbitals are occupied first. As expected from Eq. (13), the maximum anisotropy contribution is achieved at $Z=6.5$ when the bonding σ ($L_z=0$) and the bonding π ($L_z=\pm 1$) are occupied as shown in Fig. 2.

For the purpose of bringing these results about the

TABLE II. $E^{dd}(\sigma)$ per atom of the diatomic pair as a function of the occupation of the spin-down d states. Symbols $s=|V_{dd\sigma}|$, $p=|V_{dd\pi}|$, and $d=|V_{dd\delta}|$ are used for simplicity. Note that the inequalities given in column 3 hold only if $s>p>d$.

Z_d/atom	E^{dd}(PP) σ in perpendicular plane	Inequality	E^{dd}(PA) $\sigma \parallel$ pair axis
5.0	0		0
4.5	$-(\frac{1}{2}\xi)^2\left[\frac{3}{s-p}+\frac{3}{s+p}\right]$	$<$	0
3.5	$-(\frac{1}{2}\xi)^2\left[\frac{2}{p-d}+\frac{2}{p+d}+\frac{6}{s+p}\right]$	$<$	$-(\frac{1}{2}\xi)^2\left[\frac{2}{p+p}\right]$
2.5	$-(\frac{1}{2}\xi)^2\left[\frac{4}{p+d}+\frac{6}{s+p}\right]$	$>$	$-(\frac{1}{2}\xi)^2\left[\frac{8}{d+d}+\frac{2}{p+p}\right]$
1.5	$-(\frac{1}{2}\xi)^2\left[\frac{2}{p-d}+\frac{2}{p+d}+\frac{6}{s+p}\right]$	$<$	$-(\frac{1}{2}\xi)^2\left[\frac{2}{p+p}\right]$
0.5	$-(\frac{1}{2}\xi)^2\left[\frac{3}{s-p}+\frac{3}{s+p}\right]$	$<$	0
0	0		0

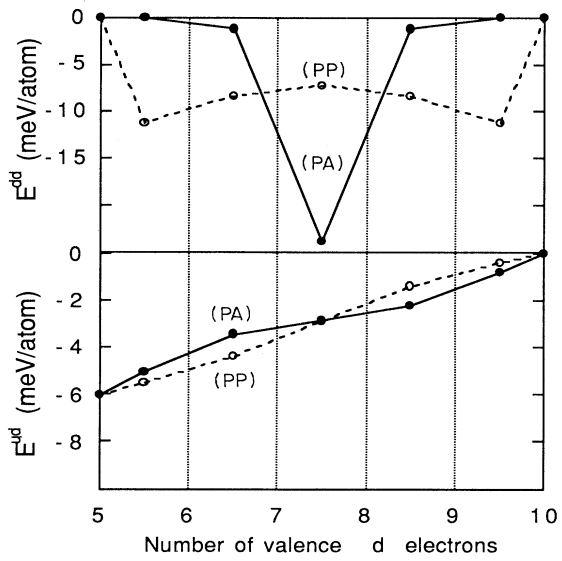

FIG. 2. The SOC energy $E^{dd}(\sigma)$ and $E^{ud}(\sigma)$ of diatomic pairs as a function of the number of d electrons. The straight lines connecting the calculated points serve only as a guide for the eyes. Bonding parameters and SOC constants used are $V_{dd\sigma}=-0.25$ eV, $V_{dd\pi}=0.18$ eV, $V_{dd\delta}=-0.04$ eV, $\xi=30$ meV, and $\Delta E_{ex}=3.0$ eV in accordance with the results for the Fe monolayer with lattice parameter $a=5.98$ a.u.

magnetic anisotropy of the diatomic SOC energy to a point of comparison with the first-principles calculation of the MCA of a square lattice Fe monolayer to be given in Sec. IV and demonstrating the effect of the structure of the neighboring atoms to the MCA energy, we consider the SOC induced energy of an atom interacting with its four neighboring atoms. Although it is easy to carry out a calculation on a cluster model (e.g., consisting of five atoms) in the same way as given above for the diatomic pair, in order to emphasize the underlying physical picture, we consider it more appropriate to display the following two effects of the surrounding atoms in a square lattice in a straightforward way.

First, consider the geometric or the symmetry property of the neighboring atoms. When the moment is along the layer normal (denoted as z), it lies in planes perpendicular to all axes of the four atomic pairs surrounding each atom, but when the moment is in the layer plane along one edge of the square lattice (denoted by x), it lies along half of the bonds but perpendicular to the other half. Hence the anisotropy of a square lattice would be decreased by a factor of 2 compared to the diatomic pair,

$$\Delta E^{**}=E^{**}(x)-E^{**}(z)=\frac{E^{**}(\mathrm{PA})-E^{**}(\mathrm{PP})}{2} . \quad (15)$$

Contributions from $**=dd$ and ud, and the total anisotropy ΔE^{sl} exhibit the same decrease due to symmetry. Dashed curves in Fig. 3 plot the results for ΔE^{dd} and ΔE^{ud} for square lattice monolayers calculated according to Eq. (15), using the same parameters as for Fig. 2.

Second, the energy levels will be changed when the atom is surrounded by more neighbors; this change depends on the number and symmetry, as well as on the atom type of the neighboring atoms. Since the present model discussion is only intended to give a qualitative understanding of the physical effects, we adopt a simple approximation to show this environmental effect when going from a diatomic pair to a square lattice. In this approximation, which holds accurately for s atoms with nearest-neighbor interaction, the level splitting broadens in proportion to the square root of the coordination number. Solid curves in Fig. 3 show the results when this effect is taken into account. It is seen that due to this band broadening, ΔE^{dd} is decreased by a factor of 2 again (four neighbors for the square lattice vs one for the diatomic pair), but ΔE^{ud} remains unchanged because it is almost independent of the band broadening. So it is seen that even in this case of very strong exchange splitting, the contribution from the SOC between opposite spins is not negligible (~ 0.5 meV/atom) compared to that from the SOC between spin-down states (~ 3 meV) estimated in this model.

In this simplified model, we put the emphasis on ideas and basic concepts that could be used to interpret the sophisticated first-principles theoretical results and experiment. In this respect, some general conclusions about the MCA of monolayers drawn from the diatomic-pair model are worth noting since they are almost independent of the specific choice of parameters.

(i) Different behavior is exhibited for the band filling dependence of the two MCA contributions, ΔE^{dd}, the contribution from the SOC between spin-down states,

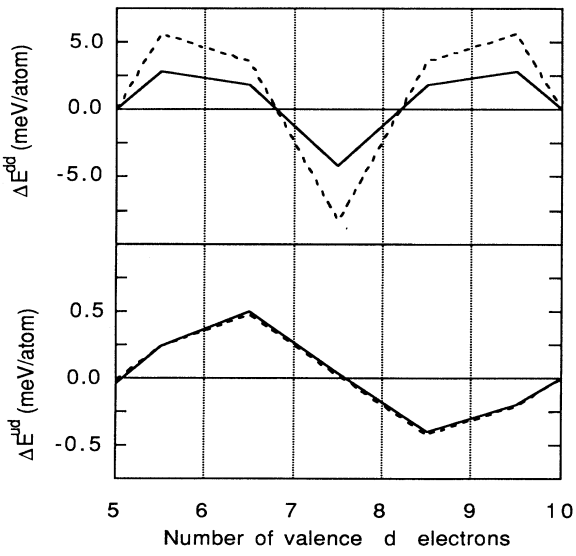

FIG. 3. The anisotropy contributions ΔE^{dd} and ΔE^{ud} calculated for a square lattice according to the diatomic-pair model. Dashed curves: only geometry (symmetry) is considered; solid curves: both geometry (symmetry) and band broadening (proportional to square root of the coordination number) are considered. Bonding parameters used are the same as in Fig. 2.

and ΔE^{ud}, the contribution from the SOC between opposite spin states, as expected from the general discussion given in Sec. II.

(ii) The ΔE^{dd} contribution favors an easy magnetic direction in the layer plane when the spin-down d band is nearly half full, but along the layer normal at the start or at the end of the band filling.

(iii) The magnitude of ΔE^{dd} is inversely proportional to the bonding strength and changes greatly with environment.

(iv) The ΔE^{ud} contribution prefers an easy magnetic direction along the layer normal if the spin-down band is less than half full, but prefers the layer plane when the spin-down d band is more than half full.

(v) The magnitude of ΔE^{ud} depends mostly on the exchange splitting and is less sensitive to the environment.

One point omitted so far is the problem of the SOC between degenerate states, a shown in Fig. 1 by short vertical lines on the degenerate levels; the SOC exists for all four degenerate states when σ is along the pair axis. In the above discussion, the expressions in Table II and the data used to plot Figs. 2 and 3 are given for seven discrete electron occupation values when each pair of degenerate states is either occupied or empty. Thus, the coupling between these two degenerate levels does not appear in the summation given in Eq. (5). In fact, when the electron number is between these numbers (i.e., E_F falls on one level, especially on degenerate ones), and even though the physical mechanism is the same, a proper treatment has to consider the influence of the population change on the ground-state energy because the orbital angular momentum is no longer quenched for these states. A similar problem will be encountered in the band treatment at some k points where two Fermi surfaces intersect, and discussed later in Sec. IV D.

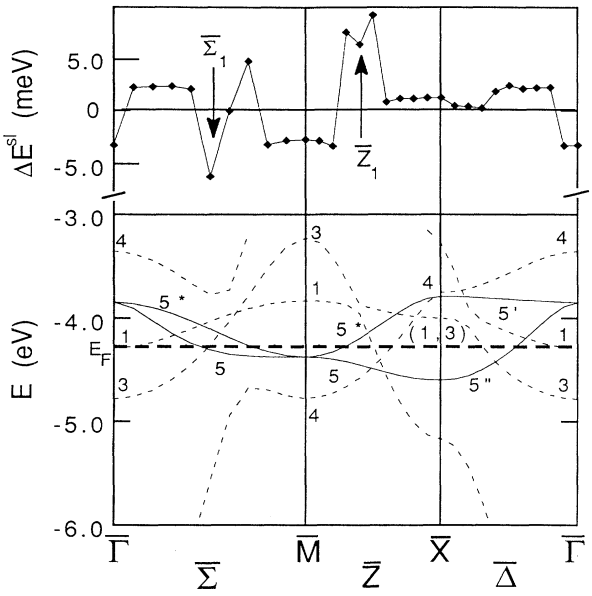

FIG. 4. The MCA contribution ΔE^{sl} from each k point vs direction in the BZ correlated with the unperturbed spin-down band of the Fe (001) monolayer ($a=5.98$ a.u.). As in Table I, 1, 3, 4, 5′, and 5″ stand for z^2, x^2-y^2, xy, yz, and xz states, respectively. Band 5 (the strongly bonding π band over most of the BZ), and band 5* (the weakly bonding or antibonding π band over most of the BZ) consisting of xz and yz orbitals, shown as solid lines, are degenerate at $\bar{\Gamma}$ and $\bar{M}$.

IV. MAGNETOCRYSTALLINE ANISOTROPY OF IRON MONOLAYERS

A. First-principles band structure

In this section, we present results for the spin polarized FLAPW band structure of Fe monolayers and the SOC shift of these states. The lattice constant is allowed to vary around the square lattice value (5.43 a.u.) of an ideal bcc Fe (001) plane by about $\pm 10\%$. For the unperturbed system, more than 100 plane waves are used as the variational basis set to solve the semirelativistic Kohn-Sham equations. Within the muffin-tin spheres, lattice harmonics with angular momentum l up to eight are used to expand the charge density, potential, and wave functions. Integrations over k space are replaced by summations over 15 special k points in the one-eighth irreducible two-dimensional BZ (100 k points in the full BZ). Convergence is assumed when the average root-mean-square deviation between the input and output charge (spin) densities is less than 2.5×10^{-4} e/(a.u.)^3.

A typical band structure is plotted in the bottom panel of Fig. 4 for the spin-down band, and Table III gives relevant levels and their spin-orbit shifts for both spin-up and spin-down bands for the monolayer with a lattice constant $a=5.98$ a.u., which matches the W (001) substrate as an example. In Table IV the SOC, exchange splitting, and bonding parameters are given for various lattice constants. The bonding parameters are determined by fitting the calculated FLAPW results to the approximate tight-binding expressions (see Table IV).

For the largest lattice constant ($a=5.98$ a.u.), the spin-down d bandwidth is about 1.56 eV. The bond strength was roughly estimated to be -0.246 eV for $V_{dd\sigma}$, 0.175 eV for $V_{dd\pi}$, and -0.040 eV for $V_{dd\delta}$. Band 3 (x^2-y^2) and band 4 (xy) orbitals lie in the layer plane; the strongest σ bonding is between them and shows the largest dispersion, distributed above and below E_F as shown in the bottom panel of Fig. 4. The band 1 (z^2) orbital lies mainly along the layer normal; it forms δ bonding and exhibits the weakest dispersion, and almost all band 1 is above E_F, except for a small bonding pocket at $\bar{\Gamma}$ where band 1 is below E_F. The area of this pocket is about 5% of the full BZ.

The xz and yz orbitals are degenerate at $\bar{\Gamma}$. The hybridization between neighboring atoms gives rise to π antibonding but δ-bonding interactions at $\bar{\Gamma}$. On the symmetry line $\bar{\Delta}$ along (100), π bonding develops for the xz orbital and gives rise to the low-lying band 5″ (see bottom panel of Fig. 4). At $\bar{X}$, the interaction between xz orbitals of neighboring atoms is of π-bonding and δ-bonding

character. By contrast, on the same $\bar{\Delta}$ line, the yz orbital keeps its π antibonding character, but only changes from δ bonding at $\bar{\Gamma}$ to δ antibonding character at $\bar{X}$. This gives rise to the high-lying band 5′. At k points along $\bar{\Sigma}$ or $\bar{Z}$ or at other general k points, xz and yz orbitals are hybridized. They always form one low-lying band 5 and one high-lying band 5*. In most of the full BZ (about 80%) where π bonding forms, the low-lying band 5 is below E_F as can be seen in Fig. 4 along $\bar{\Sigma}$, $\bar{\Delta}$, and $\bar{Z}$, while the high-lying band 5* is mostly above E_F, except in a pocket (with an area about 10% of the full BZ) around $\bar{M}$ where bands 5 and 5* are degenerate.

The exchange splitting between spin-up and spin-down bands is 2.96 eV for this Fe(001) monolayer showing a rather strong spin polarization; its magnetic moment (3.43 μ_B/atom) is much larger than the bulk value. In this case, the analysis and conclusions drawn for the limit of strong exchange splitting are expected to be the best applicable. Following rigid-band ideas, we use the density of states (DOS) calculated self-consistently for eight

TABLE III. Unperturbed states of the Fe monolayer (a=5.98 a.u.) and the spin-orbit coupling induced shifts of (a) spin-up states and (b) spin-down states. The Fermi energy is −4.275 eV.

(a) Spin-up states

k	Orbital		Energy (eV)	SOC shift (meV) $\sigma\|\|z$	$\sigma\|\|x$	
$\bar{\Gamma}$						
	4	xy	−6.536	4.1	1.9	
	(5′,5″)	(yz,xz)	−6.780	29.7	5.8	
	(5′,5″)	(yz,xz)	−6.780	−32.7	−5.6	
	1	z^2	−7.266	−1.1	−3.9	
	3	x^2-y^2	−7.273	−5.2	−3.7	
$\bar{X}$					at (100)	at (010)
	5′ or 5″	yz or xz	−6.741	−0.1	yz 4.6	xz 10.3
	4	xy	−6.810	10.4	0.2	−14.0
	(1,3)	(z^2,x^2-y^2)	−6.993	−10.8	−1.8	9.2
	5″ or 5′	xz or yz	−7.246	−2.9	xz −3.2	yz −6.6
	3	x^2-y^2	−7.437	−2.7	−5.5	−4.8
$\bar{M}$						
	3	x^2-y^2	−6.102	1.7	−1.9	
	(5′,5″)	(yz,xz)	−7.134	27.9	41.2	
	(5′,5″)	(yz,xz)	−7.134	−22.6	−1.4	
	1	z^2	−7.155	−9.8	−43.7	
	4	xy	−7.412	−3.2	−3.8	

(b) Spin-down states

k	Orbital		Energy (eV)	SOC shift (meV) $\sigma\|\|z$	$\sigma\|\|x$	
$\bar{\Gamma}$						
	4	xy	−3.353	2.6	2.9	
	(5′,5″)	(yz,xz)	−3.843	30.6	6.1	
	(5′,5″)	(yz,xz)	−3.843	−28.1	−0.6	
	1	z^2	−4.286	1.8	−3.7	
	3	x^2-y^2	−4.781	−1.2	1.4	
$\bar{X}$					at (100)	at (010)
	4	xy	−3.747	0.4	yz 8.8	xz 20.3
	5′ or 5″	yz or xz	−3.785	3.2	10.9	−8.0
	(1,3)	(z^2,x^2-y^2)	−3.997	1.4	−9.2	3.9
	5″ or 5′	xz or yz	−4.595	0.2	xz 0.1	yz −2.6
	3	x^2-y^2	−5.167	−0.3	0.5	1.5
$\bar{M}$						
	3	x^2-y^2	−3.225	2.0	1.6	
	1	z^2	−3.828	1.4	4.6	
	(5′,5″)	(yz,xz)	−4.372	27.8	2.9	
	(5′,5″)	(yz,xz)	−4.372	−24.7	−4.2	
	4	xy	−4.775	−1.2	1.1	

TABLE IV. Bonding, exchange splitting, and spin-orbit coupling parameters of Fe monolayers vs lattice constant. Bonding parameters are determined by fitting the self-consistent FLAPW results to the approximate tight-binding expression given below for a two-dimensional square lattice.

Lattice (a.u.)	Spin	Bandwidth[a] (eV)	$V_{dd\sigma}$[b] (eV)	$V_{dd\pi}$[c] (eV)	$V_{dd\delta}$[d] (eV)	ξ[e] (meV)	ΔE_{ex}[f] (eV)
5.98	up	1.17	−0.189	0.108	−0.019	31	2.96
	down	1.56	−0.246	0.175	−0.040	29	
5.73	up	1.46	−0.235	0.138	−0.026	31	2.88
	down	1.88	−0.298	0.211	−0.045	30	
5.46	up	1.86	−0.298	0.182	−0.035	32	2.86
	down	2.31	−0.365	0.266	−0.058	30	
5.24	up	2.24	−0.359	0.226	−0.044	32	2.87
	down	2.72	−0.429	0.318	−0.070	30	
4.83	up	3.28	−0.524	0.343	−0.072	31	2.82
	down	3.81	−0.609	0.437	−0.078	32	

[a]Bandwidth $= E(\bar{M}_3) - E(\bar{\Gamma}_3)$.
[b]$V_{dd\sigma} + \frac{1}{3}V_{dd\delta} = \frac{1}{6}[E(\bar{\Gamma}_3) - E(\bar{M}_3)]$.
[c]$V_{dd\pi} = \frac{1}{16}[E(\bar{\Gamma}_4) + E(\bar{\Gamma}_5) - E(\bar{X}_{5''}) + E(\bar{X}_{5'}) - E(\bar{M}_4) - E(\bar{M}_5)]$.
[d]$V_{dd\delta} = \frac{1}{8}[E(\bar{\Gamma}_5) + E(\bar{X}_{5''}) - E(\bar{X}_{5'}) - E(\bar{M}_5)]$.
[e]One-half of the spin-orbit splitting between degenerate $\bar{\Gamma}_5$ states when $\sigma \| z$.
[f]Energy difference between up- and spin-down $\bar{\Gamma}_5$ states.

electrons per Fe atom, but take the total number of electrons Z as a variable to plot the variation of the number of spin-up and spin-down electrons and their difference, i.e., the magnetic moment. Figure 5 shows the results from empty ($Z=0$) to fully filled $3d$ and $4s$ bands ($Z=12$). Since the spin-up band is lower in energy than the spin-down band due to the large exchange splitting ($\Delta E_{ex} > d$ bandwidth, for this large lattice constant), it is occupied first ($Z \leq 6$), and the magnetic moment increases with the total number of electrons, Z, in this region. The maximum moment, $5.0\mu_B$, indicates that a full occupancy of the spin-up d bands has been reached before filling the spin-down bands. When $Z \geq 6$, the increase of the number of electrons mostly falls into the spin-down d band and leads to the decrease of the net magnetic moment. The slope $dm/dZ = -0.91$, slightly less than unity, indicates that a small part of the added electrons is filling the s bands. Of course, $Z=8$ is the point of most physical importance; the number of electrons filling the spin-down d band at this point is about 1.57 as inferred from the magnetic moment if the spin polarization of the s electrons is neglected.

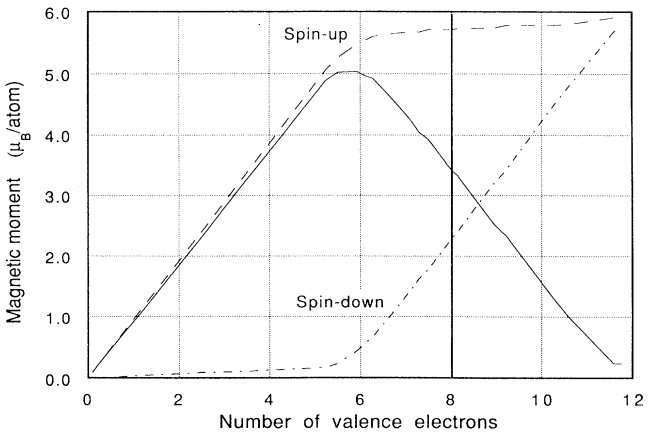

FIG. 5. Magnetic moment (solid line) and number of spin-up and spin-down electrons as a function of band filling for the Fe(001) monolayer ($a=5.98$ a.u.). The fixed self-consistent DOS for $Z=8$ is used. At $Z=8$, the magnetic moment is $3.43\mu_B$.

It is worth noting that these first-principles energy band results bear, in fact, the same feature as given in Fig. 1 for a diatomic Fe pair in the sense that the highest occupied states are the π-bonding states and the empty states belong to the δ-bonding and π antibonding states, which is of crucial importance in determining the MCA energy.

For lattice constants smaller than 5.98 a.u., the exchange splitting remains almost the same (Table IV), but the d band becomes wider due to stronger hybridization, the overlap between spin-up and spin-down bands becomes more prominent, and the separation with successive filling of both bands is not so distinctive. For the smallest lattice constant, ΔE_{ex} is less than the d-band width. Its influence on the MCA will be discussed with respect to the effect of strain in Sec. V.

While spin-up and spin-down bands have a similar structure, they are not quite the same. For example, the bandwidth and bonding strength of the spin-down band are 10–20 % larger than the spin-up band showing the nonrigid shift feature in the spin polarization and the necessity of an accurate first-principles treatment in the MCA calculations.

B. SOC induced shifts

Single-state energy shifts induced by the SOC are calculated in a second variation approach,[21,25] with all states

in the range up to 13 eV above E_F included in the variational basis. This approach contains all contributions including the higher-order terms and is thus superior to the second-order perturbation, Eq. (5). The results are given in Table III for d states at $\bar{\Gamma}$, $\bar{X}$, and $\bar{M}$. In these calculations, the SOC Hamiltonian matrix elements are given by a radial integration over the muffin-tin region, and the contributions from the interstitial and vacuum region are neglected. The degenerate unperturbed $\bar{\Gamma}_5$ states are split due to the SOC when $\sigma \| z$. This splitting equals approximately twice the SOC constant ξ if the coupling with other states is neglected. It is used as a measure of ξ and is listed in Table IV. Comparing results with different muffin-tin radii ($R_{\mathrm{MT}}=2.3$—2.9 a.u. for the lattice with $a=5.98$ a.u.) shows that ξ varies only within 1%. Thus, the neglect of the interstitial and vacuum region contributions is justified.

While the SOC strength remains almost constant for all d states, the SOC shift of different states is quite different. The largest shift happens for the coupled degenerate states, e.g., yz and xz states at $\bar{\Gamma}$ and $\bar{M}$ of either spin, when $\sigma \| z$. In this case, the shift is as large as the SOC constant itself. In other accidental quasidegenerate cases, when one state is coupled with a nearby state and their energy separation is comparable to the SOC constant, the shift could also be quite large, e.g., at $\bar{X}$ the spin-up xy and the nearby spin-up hybridized (x^2-y^2,z^2) state, with a separation of only 0.183 eV [cf. Table III (a)] are coupled through the L_z matrix element when $\sigma \| z$ and their shifts reach 10 meV. Except for these degenerate and quasidegenerate cases, the SOC shift for most states is less than 3 meV since it is a second-order effect.

These results about the spin-polarized band structure and the SOC induced single-state shift are the same as in our previous work.[21] Here, we have carried out the calculations for different lattice constants in order to study the effect of strain. In some other previous calculations, parameters such as bonding strength and SOC constants are introduced according to some empirical rule; e.g., Bruno[28] adopted Harrison's d-d bonding parameters and set $\xi=50$ meV. It turns out that this is not very far from our present accurate results, e.g., according to Harrison,[31] $V_{dd\sigma}=-0.20$ eV for Fe atoms separated by 5.98 a.u. Hence the results obtained from this kind of empirical treatment are valuable to compare with even in the quantitative sense.

C. MCA distribution in the BZ

Before presenting our results for the SOC energy calculated by using Eq. (1), which has to be summed over all occupied states and integrated over the whole BZ, it is better to first examine the contribution of each k point. This helps to build up the connection between the MCA energy and the electronic structure, and also provides an analysis and understanding of the difficulties encountered in previous theoretical treatments.

In earlier works, the MCA distribution in k space shows very strong and irregular variation. Spikes originate from the Fermi filling, and burst randomly over the BZ. The highest spike reaches as high as $\pm\epsilon$ (Ref. 20), where ϵ is the eigenvalue of the state near E_F. Note that our *state tracking method eliminates all appearances of these random contributions,* and so they do not appear in our results at all.

Results for the anisotropic part of the SOC induced energy ΔE^{sl} are shown in the top panel of Fig. 4 for k points along the high-symmetry lines for the Fe monolayer with $a=5.98$ a.u., i.e., the simplest case since its exchange splitting is much larger than the bandwidth. Comparing this curve to the band structure plotted in the bottom panel, we see the validity of the conclusion drawn from the general discussion in Sec. II that in this strong exchange-splitting limit (i) the dominant contribution comes from the SOC between spin-down (o,u) pairs and (ii) the ΔE^{sl} curve shown in the top panel of Fig. 4 can be well related through Eq. (10) to the structure of the spin-down band. For most of the full BZ where the π-bonding states (band 5) are occupied, as seen from Fig. 4, the anisotropy contribution is mostly positive because the occupied band 5 and empty band 5* are coupled through the L_z matrix element (see Table I). An exception occurs near $\bar{M}$ where both bands 5 and 5* are occupied, and the coupling between them makes no contribution to the MCA energy. By contrast, the coupling between the yz orbital of the degenerate $\bar{M}_5$ states and band 1 (z^2) through the L_x component (see also Table I) gives a negative contribution according to Eq. (10). Another small area with negative anisotropy occurs around $\bar{\Gamma}$ where band 1 (δ-bonding orbital) is occupied and both bands 5 and 5* are empty and they are coupled through the L_x matrix element. Since both negative contributions are limited around $\bar{\Gamma}$ and $\bar{M}$ to two small pockets (in total about 20% of the area of the full BZ), the positive contribution dominates the MCA energy. This demonstrates clearly the correspondence between the MCA and the band structure.

D. Surface pair coupling

There are two peaks on the curve given in the top panel of Fig. 4, however, that reflect the essential difficulties encountered in all MCA calculations. The first is in the neighborhood of $\bar{Z}_1$ (cf. top panel of Fig. 4), where bands 3, 4, 5, and 5* form (o,u) pairs mostly coupled through L_z and their energy differences are only about 0.1 eV. The second is at the $\bar{\Sigma}_1$ point where bands 5 and 3 consist of an (o,u) pair coupled through L_x and their energy difference is only 0.05 eV. In both cases, high peaks appear on the curve with positive contributions in the first case and negative in the second, because they are coupled through different angular momentum components.

These close (o,u) pairs occur in the neighborhood of the k points where two Fermi surfaces (lines for this two-dimensional case) intersect, or contact in tangency with each other. When a k point used in the BZ integration happens to be close to these intersection or tangency points and their energy separation becomes comparable to the SOC constant, the contribution of this k point to the SOC shift and the MCA becomes larger, as shown in Table III and Fig. 4. This was known for years as the problem of the surface pair coupling (SPC).[8] In the limit-

ing case, when the separation of the (o,u) pair goes to zero at a mesh point, the single-state SOC shift is proportional to the SOC constant ξ, in contrast to other k points where the shift is only a second-order effect. This leads to the singular property of the distribution of the MCA contribution in k space that plagued previous calculations.[16–23] In an integration using a finite number of k mesh points (N_k or $\bar{N}_k$ points in the full or irreducible BZ, respectively), an uncertainty of the order $\xi/\bar{N}_k$ (~ 0.3 meV, assuming $\xi=0.03$ eV and $\bar{N}_k=100$) due to SPC exists that depends sensitively on the exact location of the mesh points. Since the uncertainty is comparable to the MCA itself, the result may therefore be unreliable; for a given physical value of E_F (or total number of electrons), the resultant MCA energy will depend on the choice (not only the total number but the exact location also) of the k mesh points; equivalently, for a given set of integration points, random fluctuations occur on the MCA vs band filling curve[17,32] because the change of E_F may bring the intersections close to some k points.

However, the fact that the SPC has an effect of the order $\xi/\bar{N}_k$ on the MCA energy is not a physical property but merely an exaggeration of the use of a finite mesh integration. Physically, its effect occurs in a higher order of the SOC perturbation. First, this singularity occurs only at a very limited number of k points in the BZ, when either Fermi surfaces intersect or contact in tangency. Second, the SPC happens only in the very close vicinity of these intersection or tangency points. Assuming a linear approximation to the band dispersion in the neighborhood of this intersection point, the size of this SPC region is

$$S_{\rm spc}=\frac{\xi^2}{|\nabla_k\epsilon_o(k)\times\nabla_k\epsilon_u(k)|}\ , \tag{16}$$

if $\delta\epsilon_{uo}<\xi$ is required. With a maximum SOC shift of the order of ξ, the integrated SPC contribution is of the order of $\xi^2\times\xi$, which is at least an order higher in ξ than both the SOC energy and the anisotropy ($\propto \xi^2$ due to the reduced symmetry). Third, a proper perturbative treatment in this quasidegenerate case has to include the electron-electron interaction between states o and u. When a Hubbard term $U(1-n_o)n_u$ is included in the Hamiltonian to account for the perturbation-induced population change, then even in the exact degenerate limit ($\delta\epsilon_{uo}=0$) the change of the ground-state energy at such a k point is of the order of ξ^2/U, and the integrated contribution of an SPC region should be of order ξ^4. These effects seem to be even more important in the evaluation of the MCA contribution from the SPC region.

A natural way to take care of this problem is to increase the number of k points uniformly over the whole BZ (as was done by many previous authors) or, at the least, to increase the number of k points in the vicinity of these SPC regions.[16] Obviously, this requires too much of a computational effort and one that still leaves in doubt whether the results obtained are in the correct order of the perturbation because even with an infinite mesh integration it is still of the order of ξ^3 if the Hubbard electron-electron interaction is not included.

Our approach is to identify the existence of the SPC first by using a band filling (rigid band) calculation for varying number of valence electrons (cf. Fig. 5) in which the increment of the Fermi energy is set equal to the spin-orbit coupling strength ξ. As shown in Fig. 6(a) (to be discussed below), the SPC effect appears clearly on the band filling curve by the occurrence of random spikes with a width of a few points of Fermi energy increment and a height equal to or somewhat less than $\xi/\bar{N}_k$. Then, if the SPC singularity happens at the physical value of E_F (or Z), we believe that a better approach is to neglect entirely the contribution from this SPC region, instead of making the enormous effort to calculate its higher-order contribution. For this purpose, a decoupling approxima-

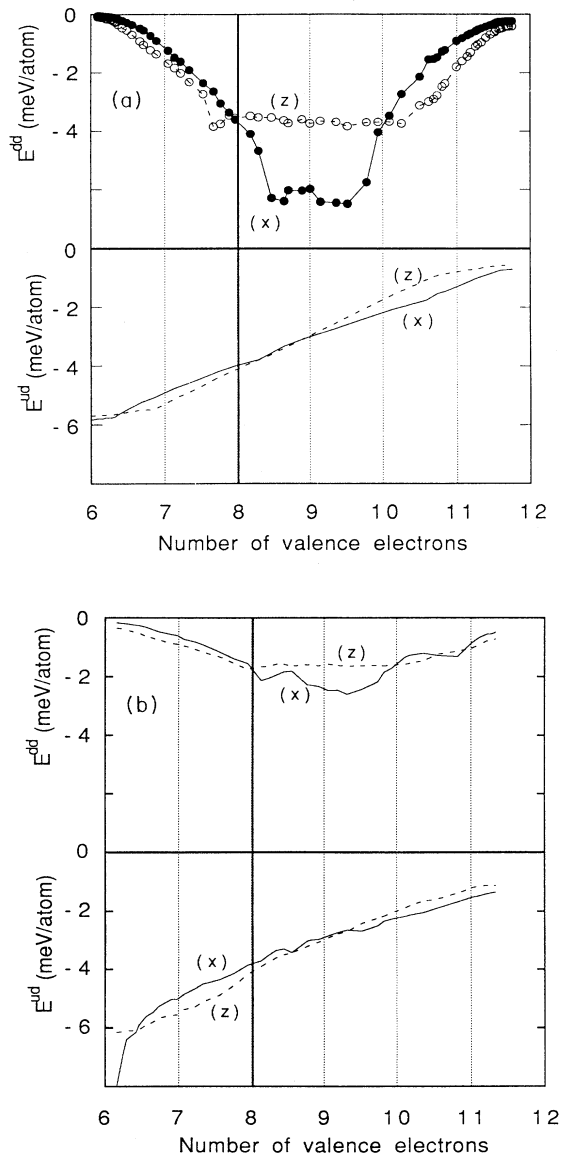

FIG. 6. The SOC energy $E^{dd}(\sigma)$ and $E^{ud}(\sigma)$ are plotted as a function of the number of electrons in the range of spin-down band filling for Fe(001) monolayers. (a) lattice constant $a=5.98$ a.u.; (b) $a=4.83$ a.u.

tion[25] has been adopted, which sets the coupling matrix element between an (o,u) pair of states at a given k point to zero when the pair is found to lie close enough to an intersection point. This reduces the uncertainties originating from the SPC singularity encountered at these k points. Such a procedure is justified from the above discussion for those systems where the second-order term dominates in their MCA energy; clearly, an extension to cubic systems requires more precise considerations.

E. SOC Energy and Magnetic Anisotropy

For calculating the change of the total energy induced by the SOC, 66 k points in the one-eighth irreducible two-dimensional BZ are employed. This corresponds to $N_k=421$ k points in the full BZ. The SOC reduced symmetry in the xy plane is considered by summing over appropriate operations for the moment direction in the plane. The state tracking method has been used to determine the SOC perturbed occupied states O'. Typical results for the SOC energy, $E^{dd}(\sigma), E^{ud}(\sigma)$, and the anisotropy are plotted against the total number of valence electrons Z in Figs. 6 and 7, using the rigid-band approximation and the DOS computed self-consistently for $Z=8$. This plot helps to reveal the SOC induced hybridization between the (o,u) states over different energy regions. Data points shown in the top panel of Fig. 6 for $E^{dd}(\sigma)$ are given for Fermi energies with an increment of 30 meV. Although the effect of the SPC occurs at a few points, e.g., on the $E^{dd}(z)$ curve at $Z=8.5$ and on the $E^{dd}(x)$ curve at $Z=7.8$, as is obviously seen, it does not influence the discussion and conclusions given below.

We consider first the SOC effect between spin-down states by turning off the SOC between opposite spins and the coupling between spin-up states. The value of $E^{dd}(z)$ and $E^{dd}(x)$ as shown in the top panel of Fig. 6 is zero at $Z=6$ or 12 (empty or fully occupied spin-down band) and reaches a maximum at half occupation where the number of SOC couplings between (o,u) states is expected to be maximum. It is worth noting that this band filling dependence bears a characteristic feature of the change of the MCA sign. When the spin-down band is nearly half filled ($Z\sim 9$), $E^{dd}(x)<E^{dd}(z)$ and ΔE^{dd} is *negative,* but when the band is at the start of band filling ($Z\sim 7.5$) or nearly fully filled ($Z\sim 10.5$), $E^{dd}(x)>E^{dd}(z)$ and ΔE^{dd} is *positive.* This means that the contribution from the coupling between spin-down bands tends to make the easy axis lie in the layer plane in the former case but to turn it to the layer normal in the latter cases.

For the contribution from the opposite-spin SOC, both $E^{ud}(z)$ and $E^{ud}(x)$ show a steady increase from -6 meV to zero with increased filling (see the bottom panel of Fig. 6). The anisotropy property of this contribution is in agreement with Eq. (13), e.g., at the start of the band filling, bonding xy and x^2-y^2 states give positive contributions, but at the central part of the band filling, negative contributions from xy, xz, and z^2 states leads ΔE^{ud} to decrease and finally, to change sign.

The MCA contributions from ΔE^{dd} and ΔE^{ud} are plotted more clearly in the center and bottom panel of Fig. 7.

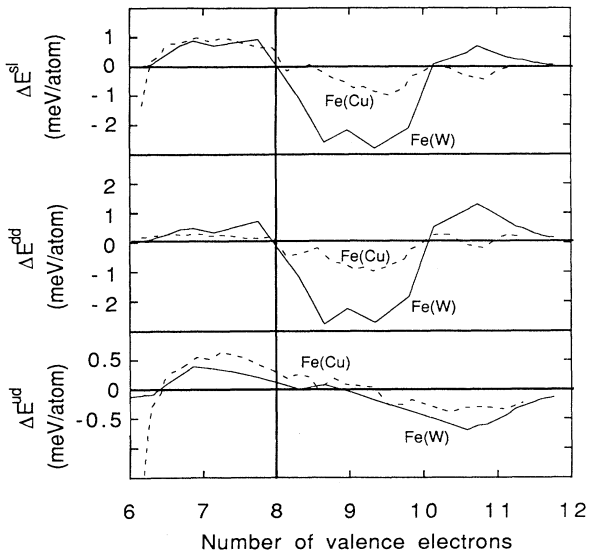

FIG. 7. The ΔE^{sl} and its two main contributions ΔE^{dd} and ΔE^{ud} of Fe(001) monolayers with lattice constant $a=5.98$ a.u. matching the W(001) substrate (solid line), compared to the monolayer with $a=4.83$ a.u. matching a Cu(001) substrate (dashed line).

It is interesting to note that the band filling dependence of the SOC energy, shown by curves $E^{dd}(\sigma)$ and $E^{ud}(\sigma)$ in Fig. 6(a), and the anisotropy for the monolayer with lattice constant $a=5.98$ a.u. shown by the solid lines in the center and bottom panel of Fig. 7, compare very well with that given in Figs. 2 and 3 for the diatomic-pair model. Surprisingly that simple model shows the correct change of MCA sign with band filling. Quantitatively, the magnitude of $E^{ud}(\sigma)$ shown in the top panel of Fig. 6(a) is in good agreement with that given for the diatomic pair (Fig. 2), but the value for $E^{dd}(\sigma)$ is about four times smaller. (Note, however, a factor of 2 could be accounted for by the band broadening due to increased coordination number.) The anisotropy contributions ΔE^{dd} and ΔE^{ud} obtained by the accurate band calculation agree with those given by the diatomic-pair model within a factor of 2. This comparison shows that although an Fe monolayer has a more complicated electronic structure and the first-principles results contain much richer phenomena, the simple diatomic-pair model still gives a good interpretation of the MCA of this two-dimensional TM system. The essence of this similarity lies in the fact that for both the diatomic-pair (Fig. 1) and the first-principles band structure (Fig. 4), the order and the occupation of the electron states are in good correspondence, i.e., their highest occupied states (bands) are the π-bonding states (bands) and the lower empty states (bands) are δ and antibonding π states (bands).

The total contribution ΔE^{sl}, which is calculated by including the SOC between all states, is plotted in the top panel of Fig. 7. It equals almost exactly the sum of the ΔE^{dd} and ΔE^{ud} contributions, in agreement with the as-

sumption that in this case of strong exchange splitting the spin-up d bands contain almost no empty states. It is also true that the contribution ΔE^{dd} shown in the center panel of Fig. 7 dominates the anisotropy ΔE^{sl} and bears the same feature of the change of MCA sign with band filling. This shows the validity of the conclusion drawn from the general discussion about the SOC energy in Sec. II that in the limit of strong exchange splitting, the coupling between opposite spin states plays a minor role since their SOC hybridization is decreased.

We have noticed a relationship between the anisotropy and the band filling (cf. Fig. 7) that there is a change of MCA sign when Z goes from ~ 7 to ~ 9. While this is an approximate curve since the DOS is calculated self-consistently only for $Z=8$, it is still worth noting because a similar relation also exists for Fe monolayers with different lattice constants (curves ΔE^{sl} in the top panel of Fig. 7). The same behavior has been found to also occur for Co monolayer films,[33] where the anisotropy constant also changes sign when Z goes from ~ 7 to ~ 9, and in that case the physical value of Z is 9 at which the anisotropy is negative. In addition, opposite signs of ΔE^{sl} have been obtained for Fe and Co by Gay and Richter[19] in their first-principles calculation for a square monolayer; Bruno[28] has also shown, in an empirical treatment of monolayer anisotropy, that the anisotropy depends on band filling and that the strongest preference for in-plane easy magnetization occurs at $Z=9$ and 9.5. Even the anisotropy constants are in approximate agreement: -3.6 meV for a square lattice with $a=5.45$ a.u. (Ref. 19), -0.5 to -2.0 meV for different choices of the crystal-field parameter,[28] and -1.35 meV for a square lattice with $a=4.83$ a.u. given in our previous paper.[33]

Our calculated angular dependence of the MCA energy fits well to a $K_2\sin^2\theta$ expression, where θ is the deviation of the moment from the layer normal.[25] The effect of terms higher than second order is negligibly small in these systems. Results for the MCA constants are listed in Table V, together with the magnetic moments for Fe monolayers with different lattice parameters. Both the easy direction and the value of the anisotropy constant are quite stable with respect to the number of k points or band filling. Even a smaller number of k points (100 in the full BZ) gives essentially the same result, when the effect of the SPC has been checked and eliminated as discussed above and reported previously.[25]

F. Comparison with experiments

Here we compare our results with the experimental findings which might test the validity of the ideas given above. Fe/Cu (100)[34] and Fe/Ag (100)[35] overlayers were found to have their easy axis along the layer normal for thicknesses below 5.7 and 2.4 MI, respectively. It was also noted that[36] besides fcc Fe (100) on Cu (100), fcc Fe (111) on Ru (0001), bct Fe (100) on Pd (100), and bcc Fe (100) on Au (100), they exhibit a perpendicular spin orientation below about 6 ML, in spite of their structural differences. This universal behavior suggests an electronic origin of this surface MCA which is consistent, at least qualitatively, with our results on Fe monolayers.

This agreement is of course very far from conclusive, however, because in the experiments the characterization of the atomic structure of these ultrathin films is especially difficult, and the MCA is shown to be crucially dependent on the local environment of the magnetic atoms. Quite aside from the difference between the experimental atomic structure of even a monolayer on a substrate and the too ideal theoretical square lattice, the interaction with substrates needs to be investigated. For example, the results for thin Co films appear controversial. Pescia *et al.*[37] found that the perpendicular remanance of thin Co overlayers (down to 1 ML) on Cu (001) was zero, but they claimed a perpendicular interface anisotropy (0.064 meV/atom) from an analysis of the deviation of the magnetization curve from the ideal demagnetization factor. Very recently, Chen *et al.*[38] found that the easy axis of a Co (2 ML) overlayer on Cu (100) is in the surface plane. Their result about Co/Cu (111) also shows that the layer normal is not the easy axis for the as-deposited films (1–3 ML); it becomes a metastable easy direction only after annealing in a magnetic field. While this seems to support the results of an in-plane MCA preference for the Co monolayers,[19,28,33] and the prediction of the change of the MCA sign depending on the band filling given above, it is evident that more studies have to be conducted.

V. EFFECT OF STRAIN ON THE MCA ENERGY OF IRON MONOLAYERS

Experimental investigations of the MCA of monolayer (or thicker) films are carried out on samples grown epitaxially on certain substrates; thus, influences on their properties may arise from the interaction between the ferromagnetic film and the substrate or from the strain induced in the epitaxy, since the lattice constants of the epitaxial overlayers may vary by several percent. For the purpose of isolating the strain effect, we have calculated the MCA energy for free-standing Fe monolayers at lattice constants that range from 11% smaller [matching the fcc Cu (001) substrate] to 10% larger [matching the bcc W (001) substrate] than the ideal iron crystal (001) surface, respectively.

The electronic states of these systems have been calculated by using our FLAPW method, as given in Sec. IV; their energy bands change greatly in the quantitative sense. For simplicity, only bonding parameters obtained by fitting our highly precise results to the approximate tight-binding expressions are given in Table IV. From the largest (5.98 a.u.) to the smallest (4.83 a.u.) lattice constant, the width of the spin-down d band increases from 1.56 to 3.81 eV. The σ bond strength $|V_{dd\sigma}|$ increases by more than twofold from 0.246 to 0.609 eV. A very good d^{-5} dependence[31] holds for $V_{dd\sigma}$. The ratios $|V_{dd\pi}|/|V_{dd\sigma}|$ and $|V_{dd\delta}|/|V_{dd\sigma}|$ remain rather stable at 0.71–0.74, and 0.13–0.16, respectively. The exchange splitting $\Delta E_{\rm ex}$ and spin-orbit coupling constant ξ remain almost constant, again showing that they are mostly an atomic property.

Figure 6(b) shows the results for an Fe monolayer with the smallest lattice constant ($a=4.83$ a.u.). Comparing it with Fig. 6(a), the $E^{dd}(\sigma)$ is greatly reduced to less than one-half of that for the largest constant monolayer ($a=5.98$ a.u.), in accordance with the increase in the bond strength. Its anisotropy contribution ΔE^{dd} shows qualitatively the same change of sign with respect to the band filling, but is also greatly reduced as can be seen from the curves in the center panels of Fig. 7. However, this change does not contribute much to the strain effect of the MCA of the Fe monolayers, because at $Z=8$, ΔE^{dd} is nearly zero (cf. the curves of the two lattices shown in the center panel of Fig. 7 pass through zero at $Z=8$).

Surprisingly, we found the MCA contribution from the SOC between the opposite spin states to be quite important in determining its strain effect. The SOC energy $E^{ud}(\sigma)$ shows a similar change with band filling for the two lattices shown in Figs. 6(a) and 6(b). Even the magnitude is almost the same, because the exchange splitting remains constant for all lattices (cf. Table IV). However, for the smallest lattice constants, almost the whole anisotropy curve ΔE^{ud} (dashed line from $Z=7$ to 11) has been shifted upward by about 0.2–0.3 meV to more positive MCA. We found that this is related to the crystal-field effect which makes the center of gravity of the bands of the planar orbitals (xy and x^2-y^2) shift to lower energy than the z^2, xz, and yz bands. The smaller the atomic spacing, the stronger this effect is expected to be. In the present case, the planar orbits of the monolayer with $a=4.83$ a.u. are found to shift 0.15 eV downward compared with the monolayer with $a=5.98$ a.u. From the change of the magnetic moment (Table V), we know that there are 0.39 more electrons to fill the down-spin band for the contracted lattice. Due to this crystal-field effect, most of these electrons fill the planar orbitals and thus push the ΔE^{ud} curve upward. [Note that each electron in these planar orbitals gives a positive contribution of about 0.9 meV according to Eq. (13).] This analysis is opposite to a simplistic assertion that might be drawn from the negative slope of the band filling curve ΔE^{ud} vs Z (see the bottom panel of Fig. 7) that an increase in the number of electrons may be accompanied by a shift of the anisotropy to more negative values. Again the conclusion is proved that the MCA is determined not only by how many states are occupied, but even more importantly, by also which states are occupied. Bruno[28] showed the effect of the crystal field by assigning a parameter in his empirical treatment; here we show how it is realized in a physical system.

A positive MCA is found for all monolayer Fe films independent of the lattice constant. The MCA constant listed in Table V for different lattice constants ranges from 0.27 to 0.42 meV/atom. As a general trend, it increases slightly with decreasing atomic spacing, but the variation is not very large. This shows that for Fe monolayers, the SOC between opposite spin states dominates in determining the effect of strain.

The results for two spacings ($a=5.45$ and 4.83 a.u.) agree approximately with the pioneering results of Gay and Richter,[18–20] which had to be computed by using as many as 7744 to 14 400 k points in the full BZ in order to obtain stable results. That the uncertainties from band filling and SPC can produce different results can also be seen from Table V by comparing with the results of Ref. 21. While no experimental comparisons can be made directly at present, our results about the effect of strain do afford an estimate as to what extent and how the lattice mismatch could influence the experimental results on the MCA.

VI. CONCLUSIONS

With the monolayer as an example, our work has proved that, when the second-order effect dominates the MCA contribution due to reduced symmetry, the MCA energy may be well related with its electronic structure. The problem of random errors introduced by the separate determination of the unperturbed and the SOC perturbed occupied states in the perturbation treatment existing in previous first-principles theoretical approaches was elim-

TABLE V. The MCA constant K_2 (in meV/atom) defined by $E^{sl}=E_0+K_2\sin^2\theta$ and magnetic moment m (in μ_B/atom) for free-standing Fe monolayers vs lattice constant taken to match the substrate shown in parentheses.

Lattice constants (a.u.)	This work		Previous work	
	K_2	m	K_2	m
5.98 (W)	0.27	3.43		
5.73 (V)	0.41	3.36		
5.45 (Ag)	0.37	3.22	0.38[a]	3.20[a]
			−0.033 to −0.043[b]	3.11 to 3.13[b]
5.24 (Pd)	0.34	3.20		
4.83 (Cu)	0.42	3.04	0.61[c]	

[a]Reference 18.
[b]Reference 21.
[c]Reference 20.

inated by employing the state tracking method which determines the SOC perturbed occupied states by their wave function with respect to the unperturbed states. This ensures that reliable physical conclusions could be drawn with respect to the MCA energy. The uncertainty from the singular property of the MCA contribution from the SPC region (in a finite mesh integration) can be identified on the band filling curve of the SOC energy and reduced, when necessary, by a decoupling approximation based on the estimate that this contribution occurs in higher-order perturbation. Quite importantly, stable results were obtained with acceptable accuracy in the first-principles calculations even with a rather limited number of k points.

The results on Fe monolayers demonstrate that there are two contributions to the MCA, from the SOC between spin-down states and between opposite spin states, which have to be taken into consideration in the theoretical treatment. Both contributions show a close relationship to the electronic structure. The contribution from the SOC between spin-down states depends strongly on the splitting and the coupling between the occupied and empty states; it is usually larger, especially in the limit of strong exchange splitting where it dominates. A change of the MCA sign is expected, depending on the spin-down band filling. This gives an explanation to the *positive* (perpendicular) MCA for Fe monolayers, and the *negative* (in-plane) MCA for free-standing Co monolayers. The predicted *positive* (perpendicular) MCA of Fe monolayers for a large range of lattice strain is in apparent agreement with experiments to date.

The contribution to the MCA from the SOC between opposite spin states exhibits characteristic band filling features. Its sign is determined by the axial component of the orbital angular momentum of the occupied states; its magnitude depends on the exchange splitting. The increase in the number of spin-down electrons for a contracted lattice is found to fill mostly the downward shifted xy and x^2-y^2 bands due to the shift of the center of gravity of these bands (crystal-field effect). This leads to more positive MCA through the contribution from the SOC between opposite spin states.

An analysis based on the bonding character of a diatomic pair, the geometry (symmetry), and the band broadening effect of the environment, is found to give a very good interpretation to the MCA energy of Fe monolayers. This reveals that the MCA of thin films (surface MCA or interface MCA) and the well-known directional ordering mechanism of the MCA of alloys may be considered on the microscopic scale through similar electronic structure studies.

ACKNOWLEDGMENTS

We thank S. Bader and C. Liu for helpful comments on this manuscript. Work at Northwestern was supported by the National Science Foundation (Grant No. 91-17818 and DMR 89-06935 and a grant of computer time at the Pittsburgh Supercomputing Center through its Division of Advanced Scientific Computing) and at Argonne National Laboratory by the Department of Energy (BES-Materials Science under Contract W-31-109-ENG-38). One of us (D.S.W.) acknowledges the support of the National Science Foundation of China.

[1]J. Kanamori, in *Magnetism,* edited by G. Rado and H. Suhl (Academic, New York, 1963), Vol. 1, Chap. 4.
[2]J. H. van Vleck, Phys. Rev. **52**, 1178 (1937).
[3]K. H. J. Buschow, in *Ferromagnetic Materials,* edited by E. P. Wohlfarth (North-Holland, Amsterdam, 1980), Vol. 1, Chap. 4.
[4]G. C. Fletcher, Proc. Phys. Soc. London **78**, 145 (1961).
[5]A. J. Bennett and B. R. Cooper, Phys. Rev. B **3**, 1642 (1971).
[6]N. Mori, Y. Fukuda, and T. Ukai, J. Phys. Soc. Jpn. **37**, 1263 (1974).
[7]N. Mori, T. Ukai, and H. Yosida, J. Phys. Soc. Jpn. **37**, 1272 (1974).
[8]E. I. Kondorskii and E. Straube, Zh. Eksp. Teor. Fiz. **63**, 356 (1972) [Sov. Phys. JETP **36**, 188 (1973)].
[9]E. I. Kondorskii, IEEE Trans. Magn. **10**, 132 (1974).
[10]N. Mori, T. Ukai, and S. Ohtsuka, J. Magn. Magn. Mater. **31-34**, 43 (1983).
[11]V. L. Morruzi, J. F. Janak, and A. R. Williams, *Calculated Electronic Properties of Metals* (Pergamon, New York, 1978).
[12]A. J. Freeman and Ruqian Wu, J. Magn. Magn. Mater. **100**, 497 (1991).
[13]L. M. Falicov, D. T. Pierce, S. D. Bader, R. Gronsky, K. B. Hathaway, H. J. Hopster, D. N. Lambeth, S. P. Parkin, G. Prinz, M. Salamon, I. K. Schuller, and R. H. Victora, J. Mater. Res. **5**, 1299 (1990).
[14]S. D. Bader, Proc. IEEE **78**, 909 (1990).
[15]H. Ekardt, L. Fritsche, and J. Noffke, J. Phys. F **17**, 943 (1987).
[16]G. H. O. Daalderrop, P. J. Kelly, and M. F. H. Schuurmans, Phys. Rev. B **41**, 11 919 (1990).
[17]P. Strange, J. B. Staunton, B. L. Gyorffy, and H. Ebert, Physica B **172**, 51 (1991).
[18]J. G. Gay and R. Richter, Phys. Rev. Lett. **56**, 2728 (1986).
[19]J. G. Gay and R. Richter, J. Appl. Phys. **61**, 3362 (1987).
[20]R. Richter and J. G. Gay, Mater. Res. Soc. Symp. Proc. **151**, 3 (1989).
[21]C. Li, A. J. Freeman, H. J. F. Jansen, and C. L. Fu, Phys. Rev. B **42**, 5433 (1990).
[22]G. H. O. Daalderrop, P. J. Kelly, and M. F. H. Schuurmans, Phys. Rev. B **42**, 7270 (1990).
[23]G. H. O. Daalderrop, P. J. Kelly, and F. J. A. den Broeder, Phys. Rev. Lett. **68**, 682 (1992).
[24]M. Weinert, R. E. Watson, and J. W. Davenport, Phys. Rev. B **32**, 2115 (1985), and references therein.
[25]D. S. Wang, R. Wu, and A. J. Freeman, Phys. Rev. Lett. **70**, 869 (1993).
[26]A. J. Freeman, C. L. Fu, Ohnishi, and M. Weinert, in *Polarized Electrons in Surface Physics,* edited by R. Feder (World Scientific, Singapore, 1985).
[27]W. Low, in *Solid State Physics,* edited by F. Seitz and D.

Turnbull (Academic, New York, 1960), Suppl. 2, p. 96.
[28]P. Bruno, Phys. Rev. B **39**, 865 (1989).
[29]P. Bruno and J. P. Renard, Appl. Phys. A **49**, 499 (1989).
[30]J. C. Slonczewski, in *Magnetism*, edited by G. Rado and H. Suhl (Academic, New York, 1963), Vol. 1, Chap. 5.
[31]W. A. Harrison, *Electronic Structure and the Properties of Solids* (Freeman, San Francisco, 1980), Chap. 20.
[32]S. Pick and H. Dreysse, Phys. Rev. B **46**, 5802 (1992).
[33]D. S. Wang, R. Wu, and A. J. Freeman (unpublished).
[34]C. Liu, E. R. Moog, and S. D. Bader, Phys. Rev. Lett. **60**, 2422 (1988).
[35]N. C. Koon, B. T. Jonker, F. A. Vokening, J. J. Krebs, and G. A. Prinz, Phys. Rev. Lett. **59**, 2463 (1987).
[36]C. Liu and S. D. Bader, J. Vac. Sci. Technol. A **3**, 2727 (1990).
[37]D. Pescia, G. Zampieri, M. Stampanoni, G. L. Bona, R. F. Willis, and F. Meier, Phys. Rev. Lett. **58**, 933 (1987).
[38]Qibiao Chen, M. Onellion, and A. Wall (unpublished).